Journal of Power Sources 196 (2011) 2461–2468

Contents lists available at ScienceDirect

Journal of Power Sources

journal homepage: www.elsevier.com/locate/jpowsour

Evaluation of carbon deposition behavior on the nickel/yttrium-stabilized zirconia anode-supported fuel cell fueled with simulated syngas

Tao Chen, Wei Guo Wang, He Miao, Tingshuai Li, Cheng Xu*

Division of Fuel Cell and Energy Technology, Ningbo Institute of Material Technology and Engineering, Chinese Academy of Sciences, 519 Zhuangshi Road, Ningbo 315201, China

ARTICLE INFO

Article history:
Received 11 November 2010
Accepted 17 November 2010
Available online 24 November 2010

Keywords:
Solid oxide fuel cell
Carbon deposition
Syngas
Degradation

ABSTRACT

The nickel/yttrium-stabilized zirconia (Ni/YSZ) anode-supported solid oxide fuel cells (SOFCs) have been operated under various simulated syngases at different temperatures to investigate the degradation behavior of the cells caused by carbon deposition. The results show that the carbon morphology and the cell performance degradation are influenced significantly by the operation temperature. The stability of the cell fueled with syngas can be improved by applying a constant current, but the cell degraded quickly after carbon deposition. The microstructure damage is close to the anode surface and leads to a conductivity decrease, which is an important reason for the cell degradation and failure at 750 °C. Conversely, the degradation behavior at 650 °C is mainly due to solid carbon deposits inside of the anode that impede fuel diffusion and electrochemical reactions on the anodic side. The effect of carbon deposition on the microstructure degradation is also investigated using transmission electron microscope.

1. Introduction

High-temperature solid oxide fuel cells (SOFCs) are a promising clean energy technology due to their high efficiency and fuel flexibility [1]. The high operation temperature allows an SOFC to operate on a large range of fuels, including hydrocarbons [2,3], coal syngas [4,5], biogas [6] and even solid carbon [7]. Among these fuels, natural gas has attracted great interest due to its convenient sources, low expense and especially its relative cleanness. The composition of natural gas, depending on the production place, is basically methane accompanied with a small amount of other hydrocarbons and a tiny amount of impurities. The natural gas can be easily reformed before utilization or can be directly oxidized into syngas in the SOFC, which can further improve the electrical efficiency of the SOFC.

Nickel/yttrium-stabilized zirconia (Ni/YSZ) cermet is the most commonly used SOFC anode material due to its catalytic effect on the electrochemical oxidation of fuel. For the cell with a Ni/YSZ anode, however, there are two major problems when fueled with a natural gas related fuel. One problem is impurity poisoning, such as sulfide, chloride and phosphide, which poisons the SOFC anode and leads to fast degradation [4,8]. The concentration of these impurities should thus be reduced to ppb levels before feeding into the SOFC. The other problem is carbon deposition because Ni is also an excellent catalyst for carbon deposition reactions, such as methane cracking (Eq. (1)), reduction of carbon monoxide (Eq. (2)) and disproportionation of monoxide (Eq. (3)). The deposited carbon can deactivate the Ni catalyst and can cause rapid cell degradation.

$$CH_4 \rightarrow C + 2H_2 \quad (1)$$

$$CO + H_2 \leftrightarrow C + H_2O \quad (2)$$

$$2CO \rightarrow C + CO_2 \quad (3)$$

Some strategies have been proposed to avoid or suppress carbon deposition in SOFCs. The investigation of the direct oxidation of natural gas suggested that the carbon deposition on a Ni/YSZ anode could be avoided by lowering the operation temperature (<700 °C) and increasing the operation current density [9,10]. These operation parameters, however, are difficult to attain in real SOFC systems. A high steam to carbon ratio (S/C) has also been used to avoid carbon deposition in the internal steam reforming of natural gas, but it reduces the cell electrical efficiency by diluting the fuel. Moreover, the strongly endothermic reforming reaction introduces excessively large temperature gradients in the stack [11,12]. Therefore, the real SOFC system usually uses an external reformer to supply syngas derived from the steam reforming of methane. The syngas derived from steam reforming consists of carbon dioxide, carbon monoxide, hydrogen, vapor and residual methane. The ratios of these compositions are determined by reforming condition and reformer design.

To solve the carbon deposition problem, many substitute anode materials have been developed to replace the Ni/YSZ cermet, including Cu–CeO–YSZ [13], doped $SrTiO_3$ [14,15], and gadolinium doped ceria [16]. However, all of these materials have obvious

* Corresponding author. Tel.: +86 574 86685139; fax: +86 574 86685704.
E-mail address: xucheng@nimte.ac.cn (C. Xu).

0378-7753/$ – see front matter © 2010 Elsevier B.V. All rights reserved.
doi:10.1016/j.jpowsour.2010.11.095

disadvantages, such as poor electrochemical catalyst activity, low conductivity, or complicated fabrication processes. The Ni/YSZ cermet is still the most preferred anode material. Therefore, it is important to understand the carbon deposition behavior on the Ni/YSZ anode, such as the prerequisite conditions for carbon deposition, and the degradation behavior of the cell due to carbon deposition.

The investigation of carbon deposition in the SOFCs with a Ni-based anode usually focuses on three issues. The first issue is the thermodynamic calculation. It is impossible to test every operation condition because different fuel compositions and operation temperatures lead to innumerable conditions; the thermodynamic calculation is thus considered a helpful tool to predict the carbon deposition conditions [17–20]. Such calculations, however, can easily deviate from real situations and require experimental verification. There are some experimental studies on this issue for certain fuels, such as the internal reforming and direct oxidation of methane [10,21].

The second issue is the deposited carbon species. Many investigations have shown that the carbon species and morphologies depend on the operation temperature and reactants. Using the technology of temperature-programmed reduction (TPR) and temperature-programmed oxidation (TPO), Finnerty et al. [22] reported that depending on the reaction temperature range, there were three carbon species from methane cracking. This result is in agreement with other research [23,24]. He and Hill [24] showed that the carbon formed at higher temperatures was bound more strongly to the catalyst surface and that the carbon morphology varied with the operation temperature. The carbon exists in the form of graphite within the SOFC operation temperature range (from 600 °C to 1000 °C), whereas the carbon nanofibers form at lower temperatures (i.e., 600 °C) and are unable to be observed at higher temperatures (i.e., 800 °C). Additionally, Alzate-Restrepo and Hill [25] investigated carbon deposition in the electrolyte-supported cells and found that the carbon formed under current was hydrogenated and easier to be removed than the carbon formed under OCV. However, it is not clear whether this effect exists in the thick Ni/YSZ cermet of the anode-supported cells.

The third issue is the degradation behavior and mechanism of the cell deposited with carbon. Understanding this issue is helpful to predict whether the carbon deposition occurs or if the performance degradation is reversible. The electrochemical impedance spectrum (EIS) usually gives detailed information about the degradation behavior due to carbon deposition. Koh et al. [26] reported the EIS change of the anode-supported cells (ASCs) fueled with methane at 750 °C. Alzate-Restrepo and Hill [27] measured the EIS of the electrolyte-supported cells (ESCs) under different CO to H_2 ratios at 800 °C. Both of their studies showed that the deposited carbon drastically increased the cell polarization (R_p) but that the carbon deposition barely had any impact on cell ohmic resistance (R_s). These results indicated that the carbon only influenced the anode function layer.

The anode cermet of the ESCs is only a catalyst layer and is very thin, so the deposited carbon should only deteriorate the cell catalyst property and increase cell polarization. Weber et al. showed that the ESCs can be operated for more than 1000 h, even when there was obvious carbon deposition [28]. The Ni/YSZ cermet for the ASC is very thick and is not only the electrochemical catalyst but also the mechanical support. The thick anode support allows for longer fuel diffusion pass, but the electrochemical reaction barely occurs. No studies have determined if carbon favors deposition on the anode functional layer. Therefore, it is necessary to know if the solid carbon has any impact on the anode support layer and especially whether the carbon deposited on the anode has an impact on mechanical properties of the cell. The present investigation was thus initiated to investigate the carbon deposition behavior on the Ni/YSZ anode-supported cell under simulated syngas to reveal the degradation mechanism of the cell due to carbon deposition.

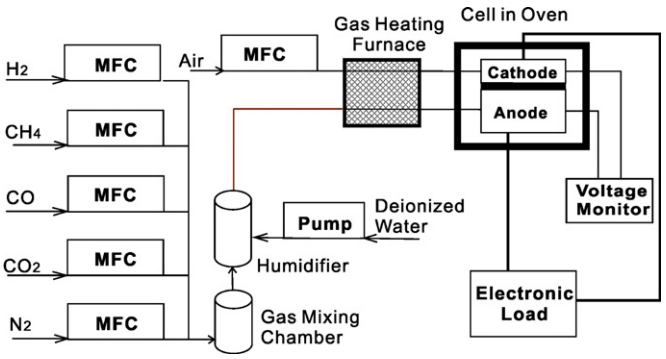

Fig. 1. Illustration of the single-cell testing system (the temperature of the red part is kept at 120 °C).

2. Experimental

2.1. Cell fabrication

The investigation was conducted using anode-supported cells produced commercially by the Ningbo Institute of Material Technology and Engineering (NIMTE), China. A 500 μm thick substrate of Ni/YSZ was tape cast as the anode support, and a 10 μm thick anode of Ni/YSZ and a 10 μm thick electrolyte of YSZ were sprayed onto the support substrate followed by sintering at 1350 °C for 3 h. A 10 μm thick cathode of 50 wt% $La_{0.75}Sr_{0.25}MnO_3$ (LSM) and 50 wt% YSZ was then sprayed on the electrolyte and fired at 1080 °C for 4 h. Prior to cell testing, a 30 μm thick current collecting layer of LSM was sprayed onto the cathode to obtain full cells. The cells used for cell testing have dimensions of $5 \times 5.8\,cm^2$ with an active area of $4 \times 4\,cm^2$.

2.2. Testing procedure

Cell testing was carried out using an identical alumina testing house. The cell was placed in the testing house and sealed with glass sealant. Ni mesh was used as the current collector on the anodic side, and Ag mesh was used as the current collector on the cathodic side. The cell was heated to 850 °C under nitrogen with a heating rate of $1\,°C\,min^{-1}$ and sealed. The anode and support were then reduced using 3% humidified hydrogen for 3 h. The hydrogen flow rate for reduction was 0.3 SLM (standard liter per minutes). The temperature was then set at 650 °C, 700 °C or 750 °C, for cell operation. The cell was operated galvanostatically at $0.63\,A\,cm^{-2}$ for at least 24 h to ensure full electrode activation [29] and stable performance under hydrogen. Then the fuel was switched to syngas at a flow of 0.5 SLM for cell endurance investigations. The syngas was obtained by mixing H_2, CH_4, CO, CO_2 and H_2O at various compositions using a commercial SOFC testing system (Bate Technology) as shown in Fig. 1. After testing, all of the cells were cooled in pure nitrogen.

The real-time current and voltage were recorded by the SOFC testing system during the process of cell testing. The electrochemical impedance spectra (EIS) were obtained with an electrochemical workstation (IM6ex, Zahner) using the four wire method before and during cell testing. The frequency range of EIS measurements was from 0.1 Hz to 100 kHz.

2.3. Microstructure examination

The microstructure of the cells both before and after testing was examined using a Hitachi S-4800 field emission scanning electron

microscope (FE-SEM). The deposited carbon was detected by an energy dispersive X-ray spectrometer (EDS) attached to the FE-SEM. For close inspection of the microstructural change of the anode during testing, the cells were carefully polished on abrasive paper to remove the cathode and electrolyte. The remainder of the cells was then ground into fine particles and observed using a Tecnai F20 transmission electron microscope (TEM).

3. Results

3.1. Thermodynamic consideration of carbon deposition

From a thermodynamic perspective, the possibility of carbon deposition can be determined if a certain operation condition is given. Therefore, the carbon deposition can be predicted by thermochemical calculations using the free energy minimization method without the details of chemical and electrochemical reactions occurring at the electrodes. There are three factors taken into account under thermochemical consideration: composition, temperature and pressure. In this study, thermochemical calculations were carried out using the HSC chemistry software (version 5, Outokumpu Research Oy, Finland).

Assuming that the initial gas amount is 100 kmol and the pressure is 1 atm, the carbon amount due to carbon deposition at different temperatures can be calculated using the free energy minimization method. Fig. 2a shows the calculation results for the cell under different simulated syngases. The amount of deposited carbon decreases with increasing temperature within the operation

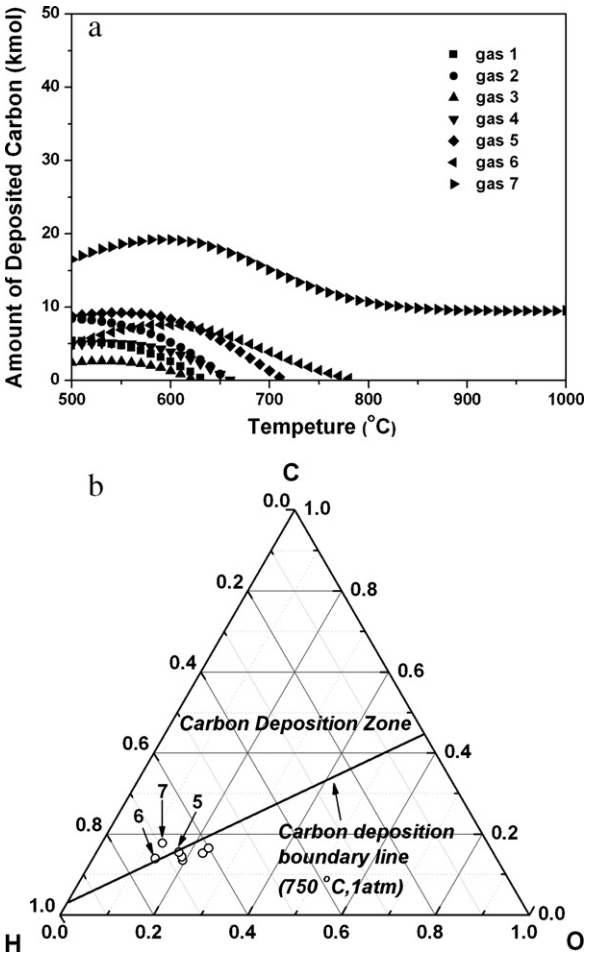

Fig. 2. Thermodynamic consideration of carbon deposition: (a) calculated carbon amount of different syngases versus operation temperature and (b) chemical equilibrium diagram of a C–H–O system at 750 °C.

Table 1
Compositions of different simulated syngases.

Number	CH_4 (%)	CO (%)	CO_2 (%)	H_2 (%)	H_2O (%)
1	0.59	10.85	18.88	64.68	5.00
2	1.64	13.25	18.67	61.44	5.00
3	3.23	5.98	18.35	67.44	5.00
4	5.51	6.88	17.90	64.72	5.00
5	9.80	7.93	17.04	60.23	5.00
6	15.09	1.91	15.98	62.01	5.00
7	23.64	7.60	14.27	49.48	5.00

temperature range of the SOFCs (600–1000 °C). Seven syngases were used in this study, and their compositions are shown in Table 1. It is apparent that the carbon deposition occurs at 750 °C only when feeding gases 6 and 7. This result can be confirmed from the C–H–O ternary diagram (Fig. 2b). Most of syngases used in this study falls in the carbon-free zone at 750 °C except for gas 7, and gases 5 and 6 approach the boundary of the carbon deposition zone.

3.2. Microstructure characteristics

Fig. 3 shows the SEM images of the anode of the cells tested under different syngases at 750 °C. The cells tested with gases 1, 2, 3 and 4 exhibit similar microstructures. A typical anodic microstructure is shown in Fig. 3a. There is no detectable structure change after cell testing, and the network of the Ni/YSZ cermet can be identified easily. For the cell exposed to gas 5 (Fig. 3b), the microstructure change is also insignificant except that the pores of the Ni/YSZ network are not as clear as the cell tested with syngas 4 (Fig. 3a). By contrast, the cell operated with gas 7 shows a drastically deteriorated morphology (Fig. 3c and d). The anode surface becomes loose, and a large number of particles appear on the surface. Fig. 3e shows the cross section of the anode of the cell operated with gas 7. Both the functional layer and the support layer exhibit the same morphology as the normal anode except for a zone with a thickness of approximately 10 μm near the anode surface. This zone can also be seen in the cell tested under gas 7 (Fig. 3f) where the surface zone is covered with carbon. It is apparent that the carbon deposition is more serious on the outside layer of the anode under these conditions.

EDS analyses were conducted on the cell surface, and the results are shown in Fig. 4. The cell tested under syngas 7 contains the largest amount of carbon on the surface, whereas no carbon can be detected for the cell tested under syngas 4. This result is consistent with thermochemical calculation result indicating that the carbon deposition occurs at 750 °C when feeding gases 6 and 7. A small amount of carbon is detected in the cell tested under gas 5. According to the C–H–O ternary equilibrium diagram, syngas 5 lies close to the boundary of the carbon deposition zone. However, the syngas may move to a non-equilibrium state due to the anode reactions and diffusion, which can lead to carbon deposition.

It is also shown that the degree of anode microstructure change relates to the amount of deposited carbon. The particles on the anode surface of the cell operated with syngas 7 marked in Fig. 3d were analyzed using EDS in Fig. 4. The results (curve d) show that Ni and C are two major compositions of the particles, which indicates that the bonding of Ni and YSZ may have been destroyed after cell testing.

Fig. 5 shows the anode microstructure of the cells exposed to gas 7 at 700 °C and 650 °C. For both cells, a large number of carbon fibers were observed in the anode surface as well as the loose particles (Fig. 5a and c). However, the amount of carbon fibers was higher in the cell tested at 650 °C than in the cell tested at 700 °C. Moreover, many carbon fibers were also found inside the anode for the cell tested at 650 °C (Fig. 5b), but they were not observed inside the cell tested at 700 °C (Fig. 5d). The results indicate that the mor-

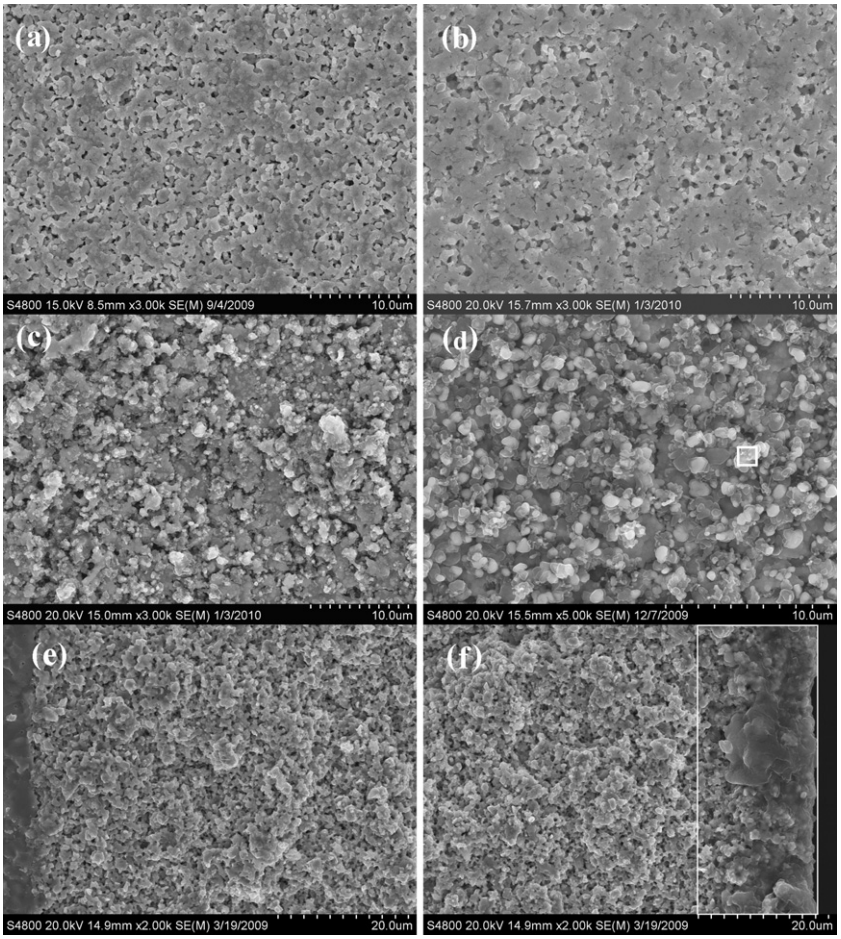

Fig. 3. Scanning electron microscope images of the cell exposed to different syngases at 750 °C: (a) surface, gas 4; (b) surface, gas 5; (c and d) surface, gas 7; (e) anode functional layer, gas 7 and (f) anode outside surface, gas 11.

phology of deposited carbon is strongly affected by the operation temperature.

3.3. Cell degradation testing

The SOFC materials and single cells have a relatively low degradation rate, i.e., <1% per 1000 h, for industrial applications. Some external factors, however, such as impurity poisoning and the redox cycle, may result in cell degradation in a short period of time [8,30]. Carbon deposition is an important factor influencing the cell stability and may cause fast degradation in the cell performance, with fuels containing hydrocarbon or carbon monoxide [28]. In this case, the cell stability is even more important than the power output. In this study, the cell stability was tested under various conditions to investigate the effect of carbon deposition on the degradation behavior of the Ni/YSZ anode-supported cell.

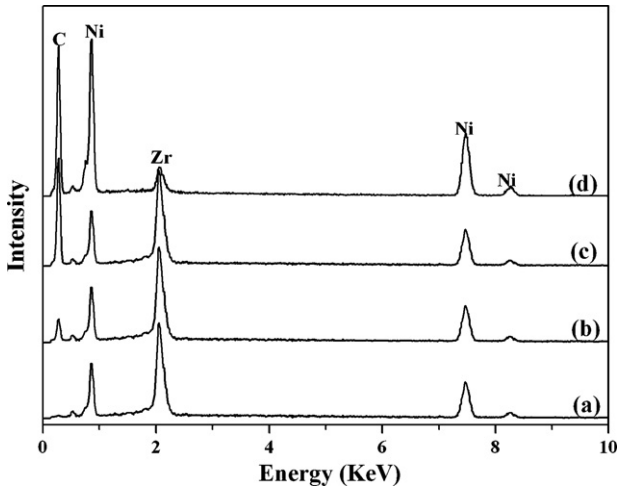

Fig. 4. EDS results for the cell surface exposed to syngas at 750 °C: (a) gas 4, (b) gas 5; (c) gas 7 and (d) gas 7, marked particles in Fig. 3d.

Fig. 6 shows the cell stability tested at 750 °C using different simulated syngases under OCV. The OCV was stable when the cell was fed with gases 1, 2, 3 and 4. These results are consistent with the thermochemical calculation results that the carbon deposition should not occur under these fuels at 750 °C. However, the OCV value dropped slightly when the fuel was switched to gases 5, 6 or 7 and then fluctuated with a tendency to decrease with increasing time. For the cells tested under gases 6 and 7, the degradation could not be reversed by switching the fuel to pure hydrogen. These cells could also not be operated under pure H_2, indicating complete failure of the cells. It has been shown above that carbon deposition can be observed at the surface of the anode of the cells tested under gases 5, 6 and 7. Therefore, the change of the OCV in Fig. 5 is mainly due to carbon deposition.

Fig. 7 shows the stability testing results under a constant current density of 0.63 A cm^{-2}. The cell was tested at 850 °C and 750 °C for 20 h under each syngas. The test was accomplished with one cell, and no detectable voltage degradation was observed for all syngases used in this investigation except gas 7. The cell performance deteriorated quickly and finally failed when feeding gas 7.

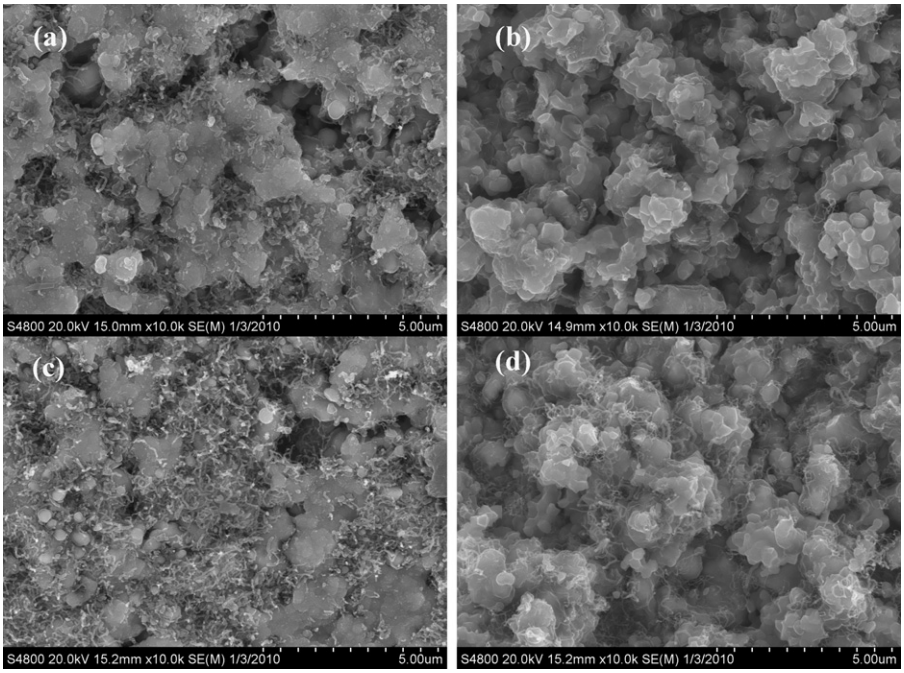

Fig. 5. Scanning electron microscope images of the cell exposed to gas 7 at 700 °C and 650 °C: (a) 700 °C, surface; (b) 700 °C, cross section; (c) 650 °C, surface and (d) 650 °C, cross section.

This result is consistent with the results in Fig. 6. However, the cell exhibited a stable voltage when feeding with gases 5 and 6, although the voltage fluctuated at OCV as shown in Fig. 6. This result may be because operation under current is helpful to suppress or avoid carbon deposition. When the cell is operated under current, the oxygen ions transport from the cathode to the anode and produce CO_2 and H_2O at the anode functional layer from electrochemical oxidation of H_2, CO and residual CH_4. The increase in the concentrations of H_2O and CO_2 is helpful to suppress carbon deposition, and thus, the carbon deposition is less favorable in the cell operated under current. In the C–H–O ternary diagram, this effect can be explained by the moving of the position of gases 5 and 6 away from the carbon deposition boundary line due to the increase of the oxygen content through electrochemical reactions. This effect can usually be identified only with relatively high fuel utilization (FU), but the FU in this study is quite low (<5%), and the effect is rather small. This result indicates that the carbon-supersaturation environments for gases 5 and 6 are sensitive to the operation condition.

Fig. 8 shows the stability testing results at different temperatures using gas 7. All of the cells were tested under gas 7 for 2 h at a constant temperature and were then switched to hydrogen fuel for regeneration. The cell tested at 750 °C showed a slow degradation rate in the beginning and then rapid performance deterioration. The voltage kept decreasing even after switching the fuel to hydrogen, suggesting the failure of the cell. The cells tested at 700 °C and 650 °C showed a quick degradation at the beginning, and the performance of the cell tested at 700 °C failed to recover after switching the fuel to hydrogen. Moreover, the OCV of the cell tested at 700 °C

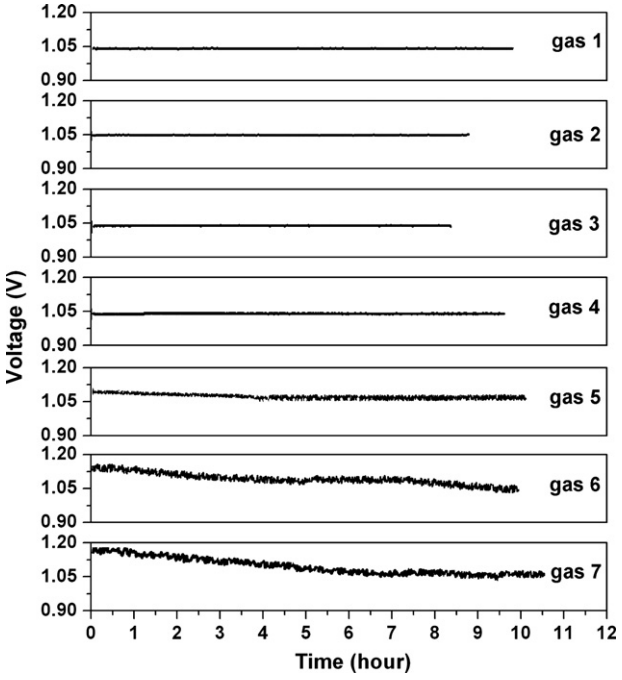

Fig. 6. OCV stability under different syngases at 750 °C.

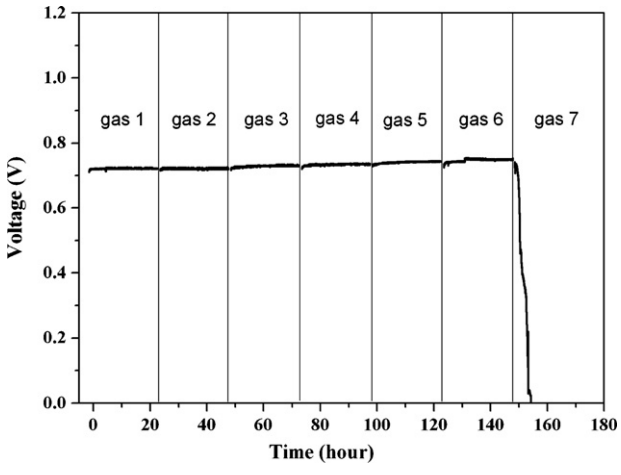

Fig. 7. Cell stability testing results at a current density of 0.63 A cm^{-2} under various syngases at 750 °C.

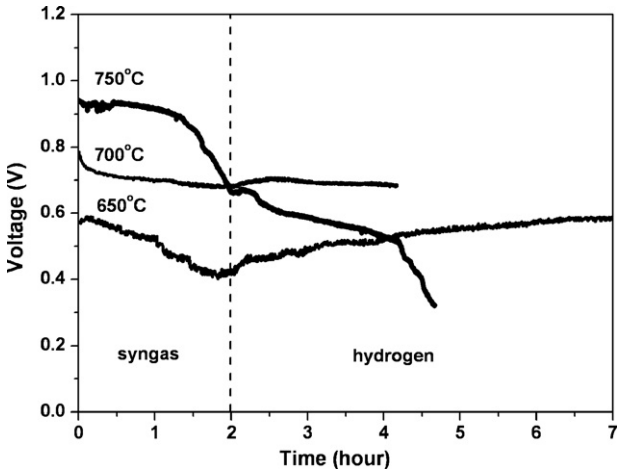

Fig. 8. Cell stability testing results at different temperatures with gas 7 (with a current density of 0.23 A cm^{-2}).

decreased from 1.105 V to 9.87 V and kept decreasing as the gas flow rate for either the fuel or air changed. In our experience, this phenomenon suggests that the electrolyte is cracked. For the cell tested at 650 °C, the performance can be recovered slowly from the degradation under syngas.

4. Discussion

4.1. Effect of carbon deposition on degradation behavior

It can be seen from degradation testing results that the cells tested at 750 °C and 650 °C have different degradation behaviors and structural changes that are related to carbon deposition. This similarity indicates that the dominant degradation mechanism may vary at different operation temperatures and is the effect of carbon deposition. Usually, electrochemical impedance spectroscopy (EIS) can provide more detailed information regarding electrode degradation behavior. Fig. 9 shows the EIS results obtained at OCV for the cell fueled with gas 7 at 750 °C and 650 °C.

Two different degradation modes can be observed in Fig. 9 for the cell tested at different temperatures. The cell tested 750 °C exhibits resistance increases both in series resistance (R_s) and polarization resistance (R_p). The increase of R_p mainly contributes to the high frequency arc, while the low frequency arc has little to do with the resistance increase. The cell tested at 650 °C shows a negligible increase in R_s but a great increase in R_p, which contributes to both the high frequency and the low frequency arcs.

The significant carbon deposition zone close to the anode surface in the cell tested under gas 7 at 750 °C (Fig. 3f) should be the reason for the increase of R_s, as shown in Fig. 10a. Therefore, the surface conductivity was measured using the four-probe method for the anode of the as-tested cell. The surface conductivity for the failed cell tested at 750 °C was only 432 S cm^{-1}, which was much less than the surface conductivity of a normal cell, approximately 1178 S cm^{-1}. The large decrease in anode conductivity due to carbon deposition on the anode surface explains the increase of R_s for the cell tested at 750 °C.

Investigations have shown that the polarization increases at the occurrence of carbon deposition because the carbon may deposit on the triple phase boundaries (TPBs) to stop the electrochemical reactions or block the pores to stop the fuel diffusion to the anode functional layer [30,31]. The anode gas diffusion process was reported [32,33] to correspond only to the low frequency arc in the impedance spectra. For the cell tested at 750 °C, however, the increase in polarization resistance is attributed to the high frequency arc, which indicates that the solid carbon deposited on the anode may not block the pores to cause fuel shortage in the anode. Although there is no obvious carbon deposition zone inside the anode (Fig. 3d and e), the solid carbon still has the possibility to deposit on the TPBs at 750 °C, which can result in the increase of high frequency part of EIS. Another possible reason for the increasing high frequency arc is that the decrease of anode conductivity may impede the charge transfer process of the electrochemical reactions.

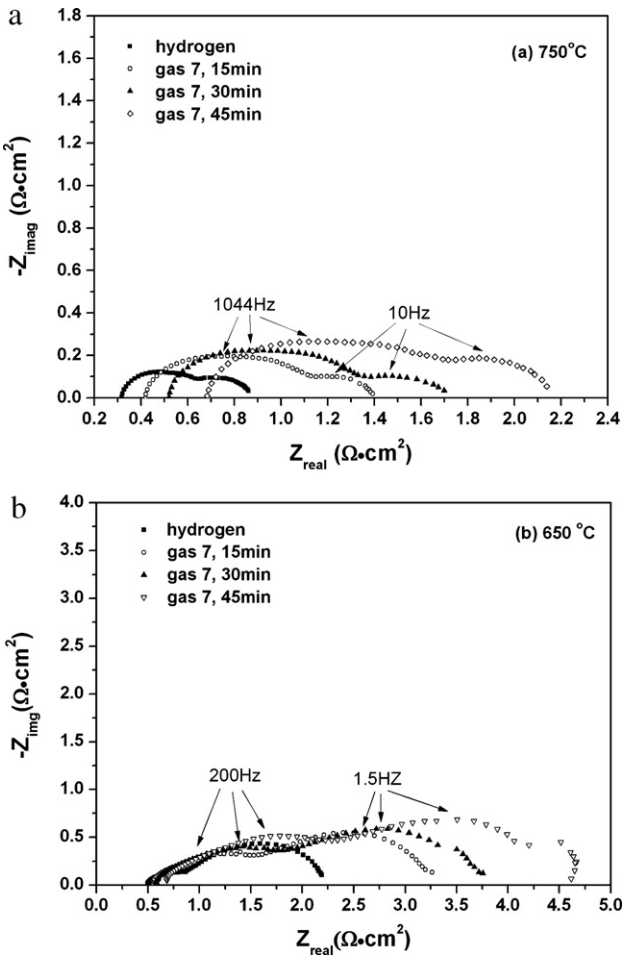

Fig. 9. EIS obtained under OCV at different time intervals at (a) 750 °C and (b) 650 °C.

For the cell tested at 650 °C, a great amount of carbon has been observed inside the anode (Fig. 5d). Therefore, the carbon may impede the fuel diffusion, which can result in an increase in the low frequency part of EIS. Furthermore, the carbon deposited on the TPBs should be responsible for the increase in the high frequency part of the EIS.

The conductivity decrease caused by anode structure damage is an important reason for the degradation caused by carbon deposition at 750 °C. Solid carbon may also deposit on the TPBs to impede the electrochemical reactions in the anode. By contrast, the degradation at 650 °C should be mainly attributed to solid carbon formed inside the anode to impede the fuel diffusion and electrochemical reactions because no significant anodic structure damage was observed and the performance degradation was partly reversible.

4.2. Effect of carbon deposition on anode microstructure at 750 °C

As discussed above, the increase of the ohmic resistance of the anode is an important reason for cell degradation when the carbon deposition occurs. This unwanted phenomenon is usually due to

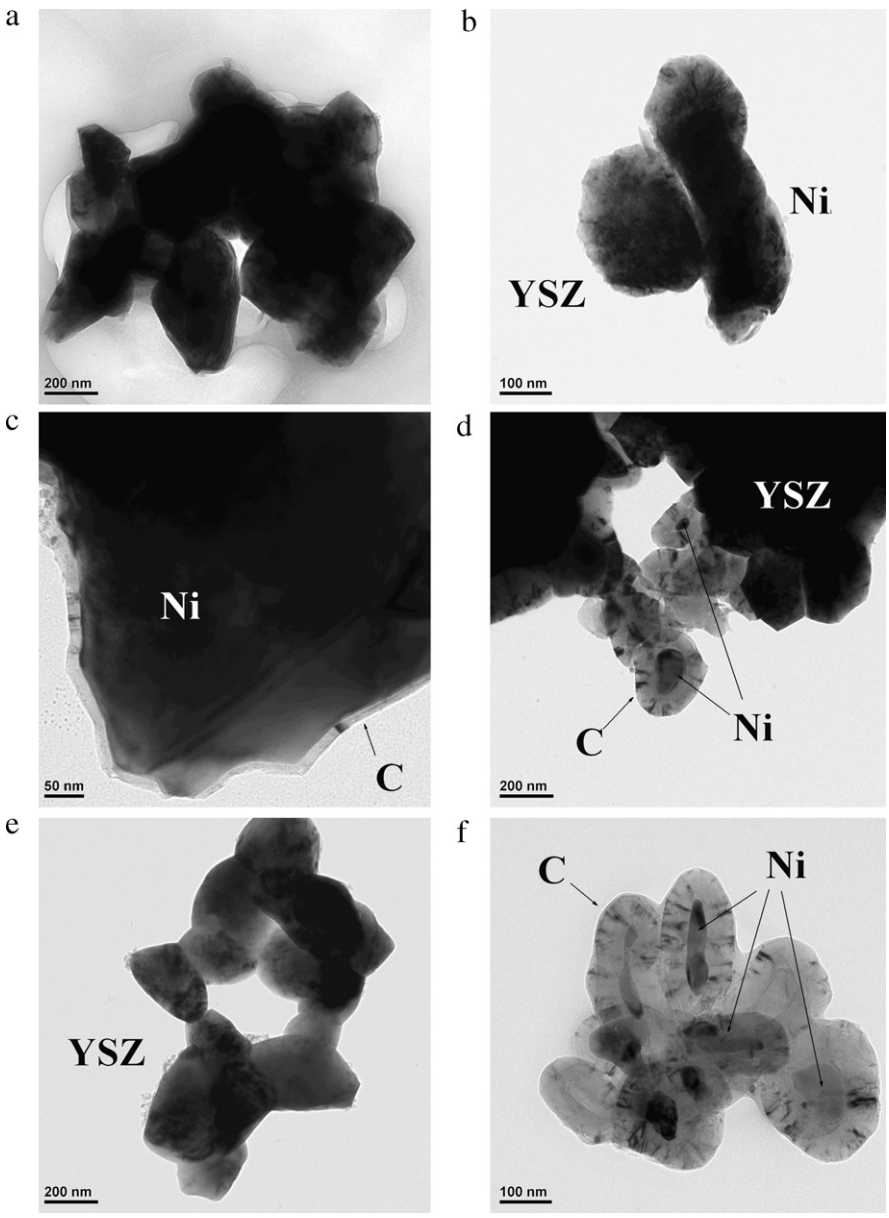

Fig. 10. Transmission electron microscope result of the anode (a and b) operated with hydrogen; (c) operated with syngas 7 for 15 min; (d–f) operated with syngas 7 for 2 h.

the formation of a new insulating phase or due to a breakdown of the Ni network. The XRD analysis for the anode of the cell tested under gas 7 showed that no new phases were detected besides graphite, nickel and YSZ. Therefore, the formation of an insulating phase such as nickel carbide may not be responsible for the ohmic resistance increase.

Further identification of the change in the anode was conducted by TEM analysis using three kinds of samples. These samples include the cell operated under humidified hydrogen, the cell operated under gas 7 for 15 min and the cell operated under gas 7 for 2 h. All of the cells were operated at 750 °C and were polished to remove cathode and electrolyte so that the investigation was focused on the carbon deposition zone approaching the anode surface. The EDX analysis was then used to identify different particles.

Fig. 10a and b shows that the cell operated under hydrogen had the anode in which the nickel and YSZ were bonded tightly even after grinding the sample into particles for TEM analysis. After 15 min of operation under gas 7 (Fig. 10c), a 10 nm thick carbon layer was observed evenly surrounding the nickel particles. The carbon layer became much thicker after exposure to syngas for 2 h, and the Ni particles became smaller (Fig. 10d and f). The Ni particles had sizes in the nanometer range and were separated from the zirconia by the carbon layer. The separated YSZ bones can also be found in the sample (Fig. 10e). This phenomenon is similar to the metal dusting effect in corrosion science.

In the metal dusting theory [34–36], pure nickel or nickel-based alloys exposed to carbon supersaturated gas at high temperatures, i.e., 800 °C, can be disintegrated into fine powders by deposited carbon. This mechanism has been validated, and it involves several microprocesses. First, the carbon deposits on the nickel and forms randomly oriented base planes on different nickel lattice planes. Second, the graphite grows into the metal through certain nickel lattice surface. Although it is not in agreement with the lattice surface in the preferred diffusion path, the only feasible driving force for carbon diffusion is provided by the difference between the supersaturated activity at the gas–metal interface and the activity of the matrix at the precipitation site [37]. Finally, the nickel disintegrates into powders after graphite penetration.

In the present investigation, the anode is 50 wt% Ni-based cermet, and some of the fuels (gases 6 and 7) are carbon super-

saturated. All of these parameters agree with the conditions for metal dusting. Moreover, the porous structure of the Ni/YSZ cermet results in a large metal surface area and a large amount of grain boundaries exposed to the fuel. This porous structure may accelerate the metal dusting because the nucleation of graphite is preferred on grain boundaries and sub-boundaries of the metal [38] according to the metal dusting mechanism.

Therefore, the impact of deposited carbon on the Ni/YSZ cermet at high temperatures (e.g., 750 °C) can be accounted for by using the metal dusting theory. According to this mechanism, the carbon deposited on the nickel can penetrate into the nickel particles and initiate the metal dusting process. The continuous dusting processes will break the contact of nickel particles, resulting in a decrease in conductivity. The metal dusting can also introduce extra stress that can lead to deformation of the anode and finally the fracture of the electrolyte. This behavior was observed in some of the failed cells in this study.

5. Conclusions

The Ni/YSZ anode-supported SOFCs were operated under various simulated syngases at different temperatures to investigate the degradation behavior of the cells caused by carbon deposition. The results showed that the carbon morphology and the cell performance degradation were significantly influenced by operation temperature. The stability of the cell fueled with syngas could be improved by applying a constant current, but the cell degraded quickly after the occurrence of deposited carbon. The microstructure damage close to the anode surface induced a conductivity decrease, which is an important factor in the cell degradation and failure at 750 °C. However, the degradation behavior at 650 °C is due to solid carbon deposits inside the anode that impede fuel diffusion and electrochemical reactions on the anode side. The Ni corrosion due to deposited carbon at 750 °C was observed and may lead to direct structural damage of the anode.

Acknowledgements

This work was conducted at the Ningbo Institute of Material Technology and Engineering at the Chinese Academy of Sciences and was financially supported by the Chinese Academy of Sciences Grant no. KJCX2-YW-H21-01 and the Zhejiang Provincial Natural Science Foundation of China Grant no. Y4100014.

References

[1] S.C. Singhal, K. Kendall, High Temperature Solid Oxide Fuel Cells – Fundamentals Design and Applications, Elsevier, UK, 2002.
[2] G.J. Saunders, J. Preece, K. Kendall, J. Power Sources 131 (2004) 23–26.
[3] S. McIntosh, R.J. Gorte, Chem. Rev. 104 (2004) 4845–4865.
[4] F.N. Cayan, M.J. Zhi, S.R. Pakalapati, I. Celik, N.Q. Wu, R. Gemmen, J. Power Sources 185 (2008) 595–602.
[5] R.S. Gemmen, J. Trembly, J. Power Sources 161 (2006) 1084–1095.
[6] J. Van herle, Y. Membrez, O. Bucheli, J. Power Sources 127 (2004) 300–312.
[7] D.X. Cao, Y. Sun, G.L. Wang, J. Power Sources 167 (2007) 250–257.
[8] T.S. Li, H. Miao, T. Chen, W.G. Wang, C. Xu, J. Electrochem. Soc. 156 (2009) B1383–B1388.
[9] Y.B. Lin, Z.L. Zhan, J. Liu, S.A. Barnett, Solid State Ionics 176 (2005) 1827–1835.
[10] J.A. Liu, S.A. Barnett, Solid State Ionics 158 (2003) 11–16.
[11] A. Gunji, C. Wen, J. Otomo, T. Kobayashi, K. Ukai, Y. Mizutani, H. Takahashi, J. Power Sources 131 (2004) 285–288.
[12] P. Vernoux, M. Guillodo, J. Fouletier, A. Hammou, Solid State Ionics 135 (2000) 425–431.
[13] S.D. Park, J.M. Vohs, R.J. Gorte, Nature 404 (2000) 265–267.
[14] S.Q. Hui, A. Petric, J. Electrochem. Soc. 149 (2002) J1–J10.
[15] J. Canales-Vazquez, S.W. Tao, J.T.S. Irvine, Solid State Ionics 159 (2003) 159–165.
[16] E. Ramirez-Cabrera, A. Atkinson, D. Chadwick, Solid State Ionics 136 (2000) 825–831.
[17] K. Sasaki, Y. Teraoka, J. Electrochem. Soc. 150 (2003) A878–A884.
[18] K. Sasaki, Y. Teraoka, J. Electrochem. Soc. 150 (2003) A885–A888.
[19] J.H. Koh, B.S. Kang, H.C. Lim, Y.S. Yoo, Electrochem. Solid State 4 (2001) A12–A15.
[20] K. Ke, A. Gunji, H. Mori, S. Tsuchida, H. Takahashi, K. Ukai, Y. Mizutani, H. Sumi, M. Yokoyama, K. Waki, Solid State Ionics 177 (2006) 541–547.
[21] C.M. Finnerty, R.M. Ormerod, J. Power Sources 86 (2000) 390–394.
[22] C.M. Finnerty, N.J. Coe, R.H. Cunningham, R.M. Ormerod, Catal. Today 46 (1998) 137–145.
[23] N.C. Triantafyllopoulos, S.G. Neophytides, J. Catal. 217 (2003) 324–333.
[24] H.P. He, J.M. Hill, Appl. Catal. A 317 (2007) 284–292.
[25] V. Alzate-Restrepo, J.M. Hill, Appl. Catal. A 342 (2008) 49–55.
[26] J.H. Koh, Y.S. Yoo, J.W. Park, H.C. Lim, Solid State Ionics 149 (2002) 157–166.
[27] V. Alzate-Restrepo, J.M. Hill, J. Power Sources 195 (2010) 1344–1351.
[28] A. Weber, B. Sauer, A.C. Muller, D. Herbstritt, E. Ivers-Tiffee, Solid State Ionics 152 (2002) 543–550.
[29] V.A.C. Haanappel, A. Mai, J. Mertens, Solid State Ionics 177 (2006) 2033–2037.
[30] H. Yokokawa, H.Y. Tu, B. Iwanschitz, A. Mai, J. Power Sources 182 (2008) 400–412.
[31] H.Y. Tu, U. Stimming, J. Power Sources 127 (2004) 284–293.
[32] R. Barfod, A. Hagen, S. Ramousse, P.V. Hendriksen, M. Mogensen, Fuel Cell 6 (2006) 141–145.
[33] R. Barfod, M. Mogensen, T. Klemenso, A. Hagen, Y.L. Liu, P.V. Hendriksen, J. Electrochem. Soc. 154 (2007) B371–B378.
[34] H.J. Grabke, Mater. Corros. 49 (1998) 303–308.
[35] E. Pippel, J. Woltersdorf, R. Schneider, Mater. Corros. 49 (1998) 309–316.
[36] H.J. Grabke, R. Krajak, E.M. MullerLorenz, S. Strauss, Werkst. Korros. – Mater. Corros. 47 (1996) 495–504.
[37] J.Q. Zhang, P. Munroe, D.J. Young, Acta Mater. 56 (2008) 68–77.
[38] J.Q. Zhang, D.J. Young, Corros. Sci. 49 (2007) 1450–1467.